THE JOURNAL OF PHYSICAL CHEMISTRY B
A JOURNAL OF THE AMERICAN CHEMICAL SOCIETY

pubs.acs.org/JPCB

Article

Dynamics of Concentrated Aqueous Lithium Chloride Solutions Investigated with Optical Kerr Effect Experiments

Stephen J. Van Wyck and Michael D. Fayer*

Cite This: *J. Phys. Chem. B* 2023, 127, 3488−3495

Read Online

ACCESS | Metrics & More | Article Recommendations | Supporting Information

ABSTRACT: We report the dynamics of concentrated lithium chloride aqueous solutions over a range of moderate to high concentrations. Concentrations (1−29 to 1−3.3 LiCl−water) were studied in which, at the highest concentrations, there are far too few water molecules to solvate the ions. The measurements were made with optically heterodyne-detected optical Kerr effect experiments, a non-resonant technique able to observe dynamics over a wide range of time scales and signal amplitudes. While the pure water decay is a biexponential, the LiCl−water decays are tetra-exponentials at all concentrations. The faster two decays arise from water dynamics, while the slower two decays reflect the dynamics of the ion-water network. The fastest decay (t_1) is the same as pure water at all concentrations. The second decay (t_2) is also the same as that of pure water at the lower concentrations, and then, it slows with increasing concentration. The slower dynamics (t_3 and t_4), which do not have counterparts in pure water, arise from ion-water complexes and, at the highest concentrations, an extended ion-water network. Comparisons are made between the concentration dependence of the observed dynamics and simulations of structural changes from the literature, which enable the assignment of dynamics to specific ion-water structures. The concentration dependences of the bulk viscosity and the ion-water network dynamics are directly correlated. The correlation provides an atomistic-level understanding of the viscosity.

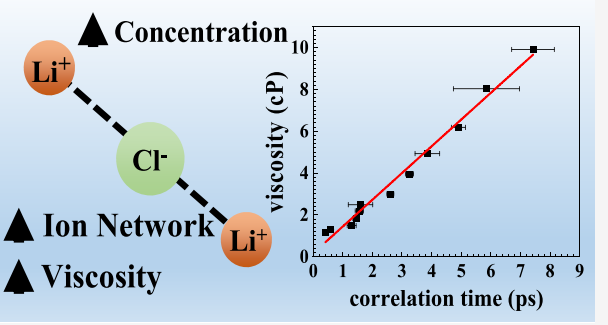

1. INTRODUCTION

The role of ions in aqueous systems is essential in chemistry, biology, and geology.[1−3] The properties of water are strongly tied to the structure and dynamics of its hydrogen bonding network. These properties have been the subject of many studies using a wide variety of techniques.[4,5] Beyond pure water, the influences of ions in aqueous solutions are subjects of a vast amount of ongoing research[6−8] and are fundamental to understanding how ion concentration affects properties such as viscosity, conductivity, and vapor pressure.[9,10]

Recently, highly concentrated "water-in-salt" electrolytes have been of interest.[11,12] In some cases, there are fewer than three water molecules per ion pair.[13,14] By mass, these systems are often primarily salt. The excess of ions changes the reduction and oxidation potentials of the water. A very high ionic mole fraction can double water's electrochemical window while still maintaining ion conductivity, which can make "water-in-salt" electrolytes attractive for applications; e.g., highly concentrated salt solution electrolytes can be a safer and more environmentally friendly battery technology. However, there remains a substantial deficit in our understanding of these systems. Theories such as Debye−Huckel can provide accurate predictions of conductivity and other properties but only for low concentrations (less than ∼0.1 M).[15] Theories that describe the complex behavior of concentrated aqueous salt solutions (great than 1 M) are lacking. This gap is a motivating factor for this research.[9]

The interactions of ions and water have been studied with numerous techniques, including nuclear magnetic resonance,[16] X-ray and neutron scattering,[17] Raman spectroscopy,[18] dielectric spectroscopy,[19−21] depolarized Rayleigh scattering,[22] and more recently ultrafast infrared (IR) spectroscopies.[23,24] These techniques provide detailed information about ion-pairing and the structure of the H-bonding network. Several recent ultrafast IR studies have focused on different aspects of highly concentrated electrolytes. Lim and co-workers studied the ultrafast dynamics of LiTFSI with concentrations up to 21 *m* by observing the anisotropy and spectral diffusion of the TFSI ion.[25] Lithium chloride has been extensively studied as a model for ionic systems.[17,20,22,26−31] LiCl's very high solubility in water makes it an appealing model for "water-in-salt" electrolytes. Recently, MeSCN was used as an IR probe molecule in ultrafast IR nonlinear spectroscopy studies of

Received: March 13, 2023
Revised: March 23, 2023
Published: April 5, 2023

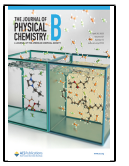

concentrated LiCl solutions. The orientational relaxation of the probe was measured, and the time dependence of chemical exchange between MeSCN-water and MeSCN-Li complexes was investigated.[32] More recent ultrafast IR investigations used the OD stretch of dilute HOD in aqueous concentrated LiCl solutions (4−6 water molecules per ion pair) to measure the details of water's orientational relaxation and structural evolution.[23]

Here, we present the results of optically heterodyne-detected optical Kerr effect (OHD-OKE) experiments on concentrated LiCl solutions. OHD-OKE is a non-resonant, probeless, ultrafast technique used to study a wide variety of systems, including room-temperature ionic liquids and aqueous ionic systems.[33−38] It reports on the dynamics of the entire system, ions, and water. We examined a wide range of concentrations from 0.06 to 0.38 ion mole fraction (29−3.3 water molecules per LiCl). We applied a tetra-exponential model to the OHD-OKE decays. We demonstrated that the data could be divided into two biexponential decays. The two fast components are associated with the dynamics of water loosely bound to contact ion pairs. The fastest component is identical to the fastest component of pure water's biexponential decay and is concentration independent. The second of the two fast components is the same as that of pure water at lower concentrations but slows at higher concentrations. The slower pair of exponentials is associated with the dynamics of ion-water complexes. As the ion mole fraction increases, the extent of the ion-water network expands, and the dynamics slow. This increased extent of the ion-water network (large ion-water complexes) and slowing were linked to the rapid, 10-fold increase in viscosity over the concentration range studied.

The results are combined with molecular dynamics (MD) simulations from the literature.[39] The simulations report that at high concentrations, as the ion mole fraction increases, the fraction of Li^+-Cl^- contact ion pairs decreases and the fraction of large complexes increases. The decrease in the ion pair fraction is identical to the decrease in the combined fractions of the two fast exponential decays, and the increase in the fraction of large ion-water complexes is identical to the increase in the combined fractions of the two slow exponentials. These results identify the sources of the experimentally measured dynamics and provide the dynamical time dependences of the structures identified in the simulations.

The observed dynamics are also able to identify the source of the concentration dependence of the viscosity. The concentration-dependent viscosities track the concentration dependence of the slow components' correlation times of the ion-water dynamics.

2. METHODS

2.1. Sample Preparation. Lithium chloride was acquired from Sigma-Aldrich (anhydrous, >99%) and used as received. The sample concentrations were prepared gravimetrically. The samples were filtered to 0.022 microns into a 1 cm glass cuvette and were sealed with a Teflon stopper. The samples were used in the experiments immediately. All experiments were performed at 24.4 °C.

2.2. Optical Kerr Effect Setup. The OHD-OKE experiment is a non-resonant, pump-probe technique, which reports on the dynamics of condensed materials. Because the OHD-OKE technique is not dependent on a probe molecule or limited by an excited state lifetime, it can explore a wide range of time scales of the pure system of interest. It provides the ground state thermal equilibrium dynamics. An intense, polarized pump pulse interacts with the sample. The oscillating electric field induces a corresponding oscillating polarization along a direction determined by the local anisotropic polarizability of the ion-water structures. The induced oscillating dipole of the medium couples to the pump pulse electric field and produces a minute alignment of the polarizability toward the direction of the pulse's electric field. The alignment causes the sample to have a small birefringence, which will decay due to the dynamics and eventual randomization of the ion-water structures. The resulting signal is the time derivative of the polarizability−polarizability correlation function.[40−42] Integration gives the polarizability−polarizability correlation function.

The OHD-OKE experimental system has been described in detail previously.[43,44] The key details are present here. Intense, short pulses were produced by a Ti-sapphire oscillator-seeded regenerative amplifier. The output pulses at 5 kHz are 80 fs with an energy of 0.2 mJ per pulse. An intense pump and weaker probe pulses were created using a 98%/2% beam splitter. The pump arrived at the sample linearly polarized, and the probe had a polarization that alternated between +45 and −45° relative to the pump. The probe is passed through crossed polarizers before and after the sample. In the simplest configuration, in the absence of the pump pulse, the sample is isotropic. Then, essentially no probe intensity would pass through the second polarizer. The pump induces a birefringence in the sample, which depolarizes the probe, permitting some of it to pass through the second polarizer, which is the signal. As the ion-water dynamics cause the induced alignment to decay, the birefringence and, therefore, the signal decay. For greater sensitivity, heterodyne detection was used. A collinear local oscillator was produced by introducing a slight ellipticity in the probe polarization. Using a Pockels cell, the ellipticity was alternated between ±3° every other shot, which is a form of phase cycling. In addition, the pump pulse polarization was alternated between 0 and 90° every two shots with another Pockels cell to reduce pump scattered light. The signal was detected with a lock-in amplifier and digitized. The result is exceptional signal-to-noise ratios over many decades of signal amplitude (4 in these experiments). The time dependence is obtained by delaying the probe pulse with a stepper motor translation stage.

The OHD-OKE data were analyzed with multi-exponential functions. For water, a biexponential was used. For all samples with LiCl, the data were fit to a tetra-exponential.

$$r(t) = R'(t) = A_1\exp(-t/t_1) + A_2\exp(-t/t_2) + A_3\exp(-t/t_3) + A_4\exp(-t/t_4) \quad (1)$$

As mentioned above, the OHD-OKE measures the time derivative of the polarizability−polarizability correlation function. The polarizability−polarizability correlation is obtained by integration of eq 1.

$$R(t) = A_1t_1\exp(-t/t_1) + A_2t_2\exp(-t/t_2) + A_3t_3\exp(-t/t_3) + A_4t_4\exp(-t/t_4) \quad (2)$$

https://doi.org/10.1021/acs.jpcb.3c01702
J. Phys. Chem. B 2023, 127, 3488−3495

Because the sign of the signal in the experiments is arbitrary, we take $R(t)$ to be positive. The prefactors in eq 2 can be normalized and relabeled in the following manner.

$$C_1 = \frac{A_1 t_1}{A_1 t_1 + A_2 t_2 + A_3 t_3 + A_4 t_4}$$
$$C_2 = \frac{A_2 t_2}{A_1 t_1 + A_2 t_2 + A_3 t_3 + A_4 t_4}$$
$$C_3 = \frac{A_3 t_3}{A_1 t_1 + A_2 t_2 + A_3 t_3 + A_4 t_4}$$
$$C_4 = \frac{A_4 t_4}{A_1 t_1 + A_2 t_2 + A_3 t_3 + A_4 t_4} \quad (3)$$

The C_i's sum to one and represent the relative proportion of each time component associated with the dynamical processes.

3. RESULTS AND DISCUSSION

3.1. OHD-OKE Decays. The source of the OHD-OKE signal is important for the following analysis. OHD-OKE measures the time derivative of the polarizability−polarizability correlation function.[40−42] The strength of the signal will be dependent on the polarizability anisotropy of the structures in the sample.[45,46] Structures that have high symmetry will yield a poor signal. As a result, the regular, tetrahedral network of water gives a weak signal. The observed weak signal for pure water results from deviations from a perfect tetrahedral structure caused by thermal fluctuations. An isolated lithium or chloride ion is a sphere. This high symmetry of a totally isolated ion (gas phase) would produce no OHD-OKE signal. The relatively strong signals observed for the LiCl solutions come from structures that are not present in pure water or in very dilute LiCl solutions. The sources of the signals are water-ion structures that have polarizability anisotropies. The lowest concentration studied is 1 ion pair per 29 water molecules (1:29). This is far from the low concentration (1 mM) at which there would be well-separated solvated ions. Even at 1:29, the ions will experience strong electric fields, and the simulations,[39] discussed below, show that there are already contact ion pair structures.

Figure 1 displays the OHD-OKE decays of a representative set of LiCl concentrations. Note the high quality of the data. The decays span amplitudes from 2.5 to 4 decades. The full set of decays is in the Supporting Information (Figure S1). Water was fit to a biexponential decay. All LiCl samples fit well to tetra-exponential decays (eq 1) with well-separated time scales. Previous OHD-OKE experiments on water by many research groups have fit the decays with biexponentials.[5,35,47−54] One group has fit the water decay with the derivative of a stretched exponential.[38,55−57] The stretched exponential model was also applied to the OHD-OKE decay of a eutectic mixture of water and LiCl, where the temperature was varied from room temperature to 130 K.[58] We were not able to achieve meaningful fits across the range of LiCl concentrations with a stretched exponential or derivative of a stretched exponential model. The multi-exponential function yielded high-quality fits (see Figure 1) and, as will be shown below, enables tracking the evolution of the dynamics across concentrations. In addition, as presented in detail below, the tetra-exponential function is consistent with concentration-dependent structural simulations of the LiCl solutions.

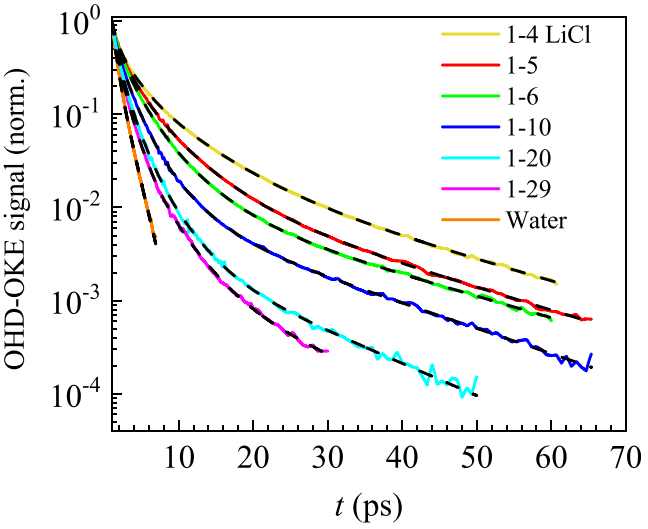

Figure 1. OHD-OKE decays of pure water and moderate to high concentrations of LiCl (solid, colored curves). The concentrations are given as 1 ion pair-number of water molecules. The dashed black curves are tetra-exponential fits to the data except for water, which is a biexponential. The decays were normalized at 1 ps.

While a tetra-exponential is a complex model for the decays, it can be broken down into two populations, each described by a biexponential decay. The first is the fast population, characterized by exponential time constants t_1 and t_2 with the corresponding correlation function amplitudes of C_1 and C_2 (eq 3). The sum of the amplitudes will be referred to as C_{fast}. The second population is characterized by slower time constants of t_3 and t_4 with amplitudes C_3 and C_4 (eq 3). The sum of these amplitudes will be referred to as C_{slow}. All four amplitudes, as well as C_{fast} and C_{slow}, are given in Table 1 for each concentration.

Figure 2 shows C_{fast} and C_{slow} as a function of the ion mole fraction. For pure water (0 ion mole fraction), it is exclusively C_{fast}. As the ion mole fraction increases, the population of C_{fast} decreases linearly, with C_{slow} increasing linearly. As discussed below, C_{fast} is associated with the dynamics of water loosely bound to contact ion pairs, while C_{slow} is associated with large ion-water complexes. At the high LiCl concentrations, the C_{slow} population begins to dominate, indicating that a large proportion of ions and water molecules is part of large ion-water complexes. The trend and relative populations are similar to data obtained using FT-IR and IR pump-probe experiments for LiTFSI.[25]

3.2. Time Constants of Dynamics. The dynamics associated with C_{fast} are also present in pure water. This is manifested in t_1 and t_2. In Figure 3A, t_1 does not change as a function of the ion mole fraction, consistently having a value of ~0.5 ps, which is within the error of pure water, 052 ± 0.03 ps (Table 2). For lower ion mole fractions, the LiCl samples' t_2's are within the error of t_2 for pure water, 1.29 ± 0.01 ps (Figure 3B and Table 2). Toward higher ion mole fractions, there is a steady slowing in t_2, reaching 2.2 ± 0.2 ps at 0.38 ion mole fraction.

The pure water decay times found here are akin to the biexponential decay times observed in 2D-IR of pure water, with similar time constants, 0.4 and 1.8 ps.[59−61] While 2D-IR and OHD-OKE measure different correlation functions, for closely related processes, the time constants would be expected to be similar. In 2D-IR of water, the fast and slow time

https://doi.org/10.1021/acs.jpcb.3c01702
J. Phys. Chem. B 2023, 127, 3488−3495

Table 1. Amplitudes of the Components of the Tetra-Exponential Decays for LiCl Concentrations

solution (ratio)	ion mole fraction	C_1	C_2	$C_{fast} = C_1 + C_2$	C_3	C_4	$C_{slow} = C_3 + C_4$
LiCl 1−3.3	0.38	0.21 ± 0.02	0.23 ± 0.01	0.44 ± 0.03	0.35 ± 0.03	0.21 ± 0.01	0.56 ± 0.03
1−3.6	0.36	0.25 ± 0.11	0.27 ± 0.07	0.53 ± 0.13	0.33 ± 0.03	0.14 ± 0.01	0.47 ± 0.04
1−4	0.33	0.23 ± 0.02	0.27 ± 0.02	0.50 ± 0.02	0.36 ± 0.01	0.14 ± 0.03	0.50 ± 0.03
1−4.4	0.31	0.24 ± 0.03	0.29 ± 0.02	0.52 ± 0.04	0.37 ± 0.03	0.11 ± 0.02	0.48 ± 0.04
1−5	0.29	0.26 ± 0.03	0.33 ± 0.03	0.58 ± 0.04	0.32 ± 0.04	0.10 ± 0.02	0.42 ± 0.04
1−6	0.25	0.29 ± 0.02	0.35 ± 0.04	0.63 ± 0.04	0.29 ± 0.07	0.080 ± 0.011	0.37 ± 0.07
1−7	0.22	0.33 ± 0.04	0.44 ± 0.05	0.77 ± 0.06	0.18 ± 0.07	0.052 ± 0.022	0.23 ± 0.07
1−8	0.20	0.35 ± 0.01	0.39 ± 0.04	0.74 ± 0.04	0.21 ± 0.04	0.045 ± 0.008	0.26 ± 0.05
1−10	0.17	0.35 ± 0.02	0.40 ± 0.03	0.75 ± 0.04	0.20 ± 0.04	0.052 ± 0.012	0.25 ± 0.05
1−14	0.13	0.39 ± 0.01	0.44 ± 0.06	0.83 ± 0.06	0.12 ± 0.06	0.052 ± 0.008	0.17 ± 0.06
1−20	0.09	0.42 ± 0.02	0.45 ± 0.01	0.87 ± 0.02	0.11 ± 0.01	0.016 ± 0.007	0.13 ± 0.02
1−29	0.06	0.47 ± 0.01	0.44 ± 0.01	0.91 ± 0.01	0.08 ± 0.01	0.009 ± 0.006	0.09 ± 0.01
water	0	0.66 ± 0.01	0.34 ± 0.01	1	n/a	n/a	n/a

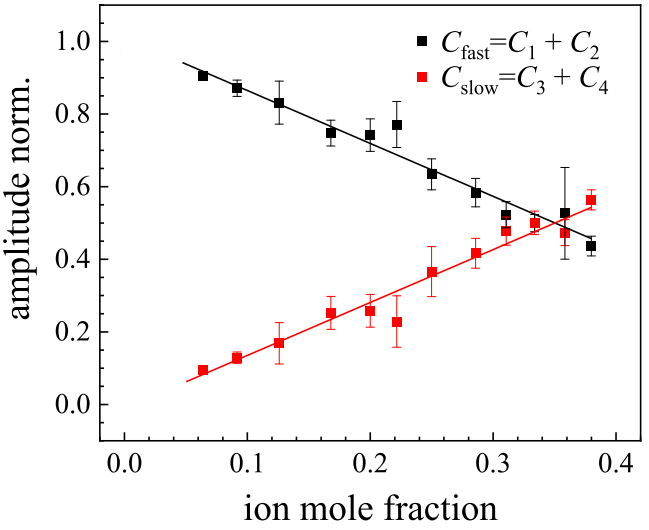

Figure 2. Amplitudes of the fast and slow portions of the decays from the coefficients of the four exponentials from the fits. $C_{fast} = C_1 + C_2$ (black points) and $C_{slow} = C_3 + C_4$ (red points). The data are plotted as a function of the ion mole fraction. The solid lines are linear fits. C_{fast} are from the decays that are closely related to those of pure water. C_{slow} come from decays associated with increasingly large ion-water clusters as the concentration is increased.

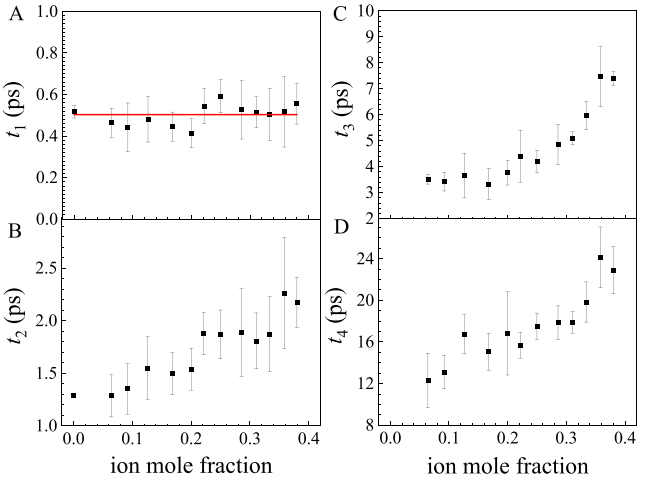

Figure 3. Time constants from the fits to the data in Figure 1. t_1 (A), t_2 (B), t_3 (C), and t_4 (D) as a function of the ion mole fraction. t_1 is the same as that found in pure water within experimental error and is independent of concentration. The other time constants become longer with increasing LiCl concentration.

constants are assigned to local H-bond fluctuations, mainly length fluctuations and the randomization of the H-bond network, respectively.[59−61] The fast time constant measured here for water-associated ions and other water molecules may be local H-bond fluctuations as in the 2D-IR experiments. However, particularly for the higher concentrations, the extended H-bond network of pure water does not exist. The second component of both measurements is likely to also arise from similar processes. The OKE data may involve reorientation, with water switching H-bonds from one anion to another as well as from one water molecule to another. Therefore, comparison to the 2D-IR results suggests that the fast OHD-OKE component arises from local H-bond fluctuations, which are independent of the LiCl concentration. The second OHD-OKE time constant is caused by the rearrangement of the water H-bonds, which slow with an increasing amount of LiCl. The slowing can occur because water becomes more entwined as the water-ion complex size grows.

The dynamics associated with C_{slow} are completely absent from pure water with time constants that are considerably slower than those found in water. Figure 3C shows that t_3 ranges from 3.5 ± 0.2 ps at 0.06 ion mole fraction to 7.4 ± 0.3 ps at 0.38 ion mole fraction (Table 2). Similarly, Figure 3D shows that t_4 is 12 ± 3 and 23 ± 2 ps for 0.06 ion mole fraction and 0.38 ion mole fraction, respectively (Table 2). These time constants reflect the decay of the polarizability−polarizability correlation function caused by the structural randomization of extended ion-water networks. As the concentration increases, these networks may become larger and therefore more constrained in their relaxation dynamics. These values are on the same order as ultrafast measurements of the frequency-frequency correlation functions of the CN stretch of MeSCN's[22] and the OD stretch of dilute HOD of the water[23] in concentrated aqueous LiCl solutions. In those experiments, dynamics sensed by a vibrational probe were measured. The dynamics reported by the probe depend on the dynamics of the ion-water structures.

3.3. Comparison to Simulations. A number of experiments and simulations have been used to investigate ion pairs and large ion-water complexes in concentrated aqueous LiCl solutions.[62,63] We compared our results to recent simulations of concentrated aqueous LiCl solutions that calculated the

https://doi.org/10.1021/acs.jpcb.3c01702
J. Phys. Chem. B 2023, 127, 3488−3495

Table 2. Tetra-Exponential Decay Time Constants and Viscosities for Aqueous LiCl Concentrations

solution (ratio)	ion mole fraction	t_1 (ps)	t_2 (ps)	t_3 (ps)	t_4 (ps)	τ_c^{slow}	viscosity (cP)[a]
LiCl 1−3.3	0.38	0.6 ± 0.1	2.2 ± 0.2	7.4 ± 0.3	23 ± 2	7.4 ± 0.7	9.9
1−3.6	0.36	0.5 ± 0.2	2.3 ± 0.5	7.5 ± 1.2	24 ± 3	5.9 ± 1.1	8.0
1−4	0.33	0.5 ± 0.1	1.9 ± 0.4	6.0 ± 0.5	20 ± 2	4.9 ± 0.2	6.2
1−4.4	0.31	0.5 ± 0.1	1.8 ± 0.3	5.1 ± 0.2	18 ± 1	3.9 ± 0.4	4.9
1−5	0.29	0.5 ± 0.1	1.9 ± 0.4	4.9 ± 0.8	18 ± 2	3.3 ± 0.1	4.0
1−6	0.25	0.6 ± 0.1	1.9 ± 0.2	4.2 ± 0.4	18 ± 1	2.6 ± 0.1	3.0
1−7	0.22	0.6 ± 0.1	1.9 ± 0.2	4.4 ± 1.0	16 ± 1	1.6 ± 0.4	2.5
1−8	0.20	0.4 ± 0.1	1.5 ± 0.2	3.8 ± 0.5	17 ± 4	1.6 ± 0.1	2.2
1−10	0.17	0.5 ± 0.1	1.5 ± 0.2	3.3 ± 0.6	15 ± 2	1.4 ± 0.1	1.8
1−14	0.13	0.5 ± 0.1	1.6 ± 0.3	3.7 ± 0.9	17 ± 2	1.3 ± 0.2	1.5
1−20	0.09	0.4 ± 0.1	1.4 ± 0.2	3.4 ± 0.4	13 ± 2	0.60 ± 0.06	1.3
1−29	0.06	0.5 ± 0.1	1.3 ± 0.2	3.5 ± 0.2	12 ± 3	0.41 ± 0.01	1.2
water	0	0.52 ± 0.03	1.29 ± 0.01	n/a	n/a	n/a	0.9

[a]Reference 64.

number of ion pairs and large ion-water complexes for a wide range of concentrations (0.11−19.28 molal).[39] MD simulations were performed with the optimized potentials for all atoms (OPLS−AA force field) and an SPC/E water model. Radial distribution functions (RDFs) were calculated for Li^+−Cl^- as a function of the concentration, which suggested the creation of contact ion pairs and potentially larger ion complexes. It was found that the RDFs obtained from the MD simulations compared favorably with X-ray and neutron scattering experiments. With increasing LiCl concentration, there were large changes in the RDFs of Li^+−Li^+ and Cl^-−Cl^-. At a low concentration (1.015 molal), there was a major peak at approximately 0.55 nm for both Li^+−Li^+ and Cl^-−Cl^-. As the LiCl concentration was increased, a new peak formed at about 0.37 nm and continued to grow with concentration. The peak was interpreted as arising from the formation of larger ion complexes as the like-charged ions require an opposite-charge ion between them. This information enabled the calculation of the percentage of Li^+ ions incorporated in ion complexes and the sorting of the ion complexes into different sizes at each LiCl concentration. The ion complexes were divided into contact ion pairs and larger ion complexes, which contained three or more ions.

The simulations found that at approximately 0.08 ion mole fraction (2.36 molal) and higher concentrations, there were a significant number of ion complexes. Figure 4A shows a comparison between the experimental C_{fast} and the simulated fraction of ion complexes that were contact ion pairs. The agreement is remarkable and provides further confirmation that C_{fast} reports on water loosely associated with contact ion pairs. With higher ion mole fractions, the proportion of contact ion pairs decreases, which is accompanied by an increase in large ion complexes. Figure 4B shows a comparison of C_{slow} with the fraction of large ion complexes as a function of the ion mole fraction. Again, the agreement between the data obtained from the measurements of the ion-water dynamics and the simulations is remarkable. At the intermediate and higher concentrations, there are insufficient water molecules to solvate separated complexes. The system is more akin to an extended ion-water network. As the fraction of extended complexes increases, the dynamics, given by t_3 and t_4, slow. These time constants reflect the dynamics of the complexes, and t_4 can be associated with the time for the structures to randomize. Figure 4 allows us to assign the time dependence of structural evolution to the ion-water complexes found in the simulations

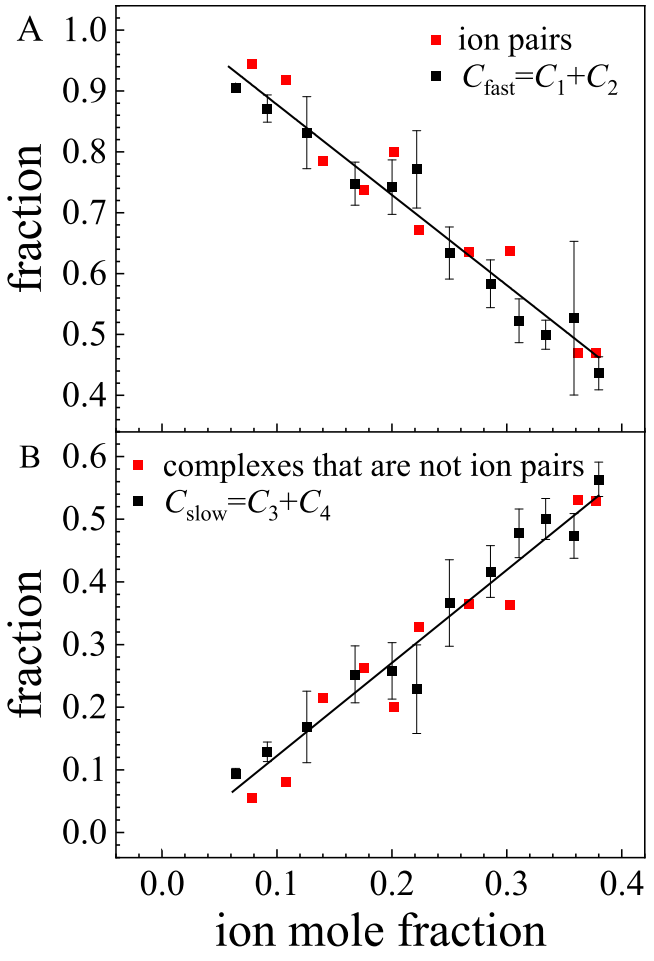

Figure 4. Comparison of the experimental data to MD simulation results from the literature.[39] (A) Fraction $C_{fast} = C_1 + C_2$ (black points) and the fraction of contact ion pairs from the simulations (red points) as a function of the ion mole fraction. (B) Fraction $C_{slow} = C_3 + C_4$ (black points) and the fraction of large ion-water complexes (not contact ion pairs) from the simulations (red points) as a function of the ion mole fraction. The lines are concatenated linear fits to the experimental data and the simulation data. The agreement between the experimental and simulation data is striking.

as a function of concentration. In addition, the concurrence of the coefficients of the exponentials measured in the experiments and the fractions of the structures obtained in the

https://doi.org/10.1021/acs.jpcb.3c01702
J. Phys. Chem. B 2023, 127, 3488−3495

simulations is strong support for the accuracy of the simulations.

3.4. Viscosity and Ion-Water Network Dynamics. The results presented above gave a detailed picture of the concentration dependence of ion-water structural dynamics at the atomistic level. The results can also be used to explicate the nature of bulk properties, in particular the viscosity, as a function of concentration.

By observing how the time constants associated with C_{slow} change with the ion mole fraction, the evolution of the ion-water network was tracked. At the lowest concentration (0.06 ion mole fraction), large ion-water complexes accounted for less than 10% of the complexes and had time constants of 3.5 ± 0.2 and 12 ± 3 ps for t_3 and t_4, respectively. As the amount of LiCl increased, the proportion of large ion-water complexes and their time constants steadily increased. For 0.38 ion mole fraction, large ion-water complexes make up 54% of all complexes, and the time constants have basically doubled to 7.4 ± 0.3 and 23 ± 2 ps for t_3 and t_4, respectively, compared to 0.06 ion mole fraction. Like the simulations,[39] these experimental changes reflect the growth of a more connected ion-water network.

Increased concentration, which is associated with the growth of the ion-water networks and the slowing of the water dynamics, coincides with the rapid increase in viscosity. We can compare the increase in the correlation time of the dynamics of the large ion-water complexes with increasing concentration to the concentration dependence of the viscosity. The correlation time is a single time constant, τ_c, that reflects the overall time scale of a combination of dynamical processes.

$$\tau_c = \int_0^\infty f(t)\mathrm{d}t \tag{4}$$

For a multi-exponential

$$\tau_c = \int_0^\infty f(t)\mathrm{d}t = \int_0^\infty \sum_i C_i e^{-t/t_i}\mathrm{d}t = \sum_i C_i t_i \tag{5}$$

The correlation time for the dynamics of the large complexes (t_3 and t_4), τ_c^{slow}, is

$$\tau_c^{slow} = C_3 t_3 + C_4 t_4 \tag{6}$$

Figure 5 shows the viscosity as a function of the correlation time, τ_c^{slow}. The red line is a fit to the data. The viscosity linearly tracks the correlation time τ_c^{slow} within experimental error. It should be noted that viscosity does not track the individual time constants, neither t_3 nor t_4. Therefore, the relationship shown in Figure 5 is not simply hydrodynamic behavior as given by the Stokes−Einstein−Debye equation. The correlation between the viscosity and τ_c^{slow}, displayed in Figure 5, demonstrates that the increase in viscosity with concentration is caused by the increase in extended ion-water structures. As the amount of water decreases, the ion-water network becomes more tightly interwoven, and the structural relaxation slows. Viscosity is a bulk property that depends on the underlying structure and dynamics of the liquid. Here, we have shown which structures of the concentrated ion-water system control the viscosity and the actual structural relaxation times that are associated with the structures.

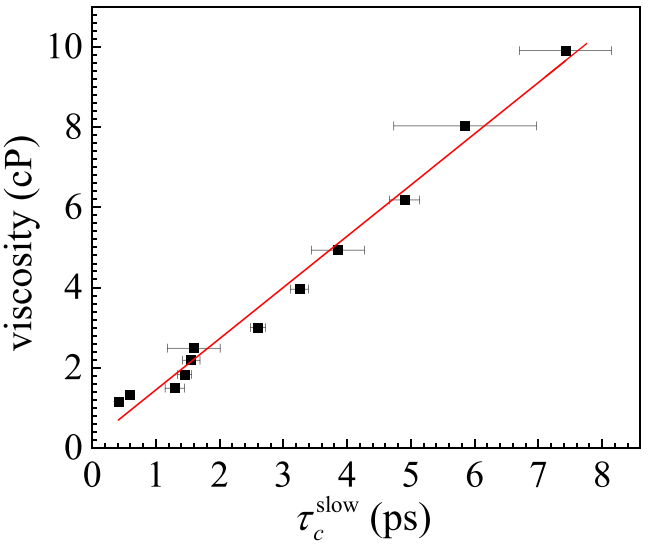

Figure 5. Viscosity plotted against the correlation time of the slow dynamics, τ_c^{slow}. The solid red line is a linear fit. The correlation between the increasing viscosity and the increasing correlation time of the slow dynamics shows that the viscosity is determined by the dynamics of the extended ion-water clusters, which slow as the amount of water decreases. The viscosity data are from ref 64.

4. CONCLUDING REMARKS

The dynamics of concentrated salt solutions and the relation of dynamics to the structure of ion-water systems are challenging problems. Here, we have presented a study of the dynamics of LiCl solutions from moderately high to very high concentrations. At the lowest concentration studied, 1 ion pair to 29 water molecules, there are a sufficient number of water molecules to solvate the ions. However, this concentration is far from the low concentration, and there are already ion pairs and larger ion complexes as shown by the experimental results. At the highest concentration, 1 ion pair per 3.3 water molecules, there are not nearly enough water molecules to fully solvate the ions. The fraction of large ion-water clusters in the extended network has become dominant.

We employed OHD-OKE experiments to measure the dynamics as a function of concentration over a broad range of time scales. There are four dynamical time scales, while pure water only has the faster two. The fastest, t_1, is identical to that of pure water. It is independent of concentration and corresponds to hydroxyl H-bond length fluctuations for water molecules solvating ion pairs. The second time constant, t_2, is identical to that of pure water at the lower concentrations but slows at higher concentrations. This time constant is likely associated with water H-bond rearrangement for water that is not trapped in the large complexes. The slower two time constants, t_3 and t_4, have no counterparts in pure water. These are substantially slower than the dynamics found in pure water. The time constants become longer, and their amplitudes increase as the concentration of ions is increased. The time constants and amplitudes arise from the dynamics of large ion-water complexes and the extended ion-water network. t_3 and t_4 are the time scales for ion-water aggregates to undergo structural change.

The assignments of the time constants can be made by comparison to the time constants of pure water and the inverse concentration dependences of the fraction of the t_1 and t_2 components, C_{fast}, versus the fractions of the t_3 and t_4

https://doi.org/10.1021/acs.jpcb.3c01702
J. Phys. Chem. B 2023, 127, 3488−3495

components, C_{slow}, as shown in Figure 2. The relation of the dynamics and structure is strongly supported by MD simulations from the literature.[39] The simulations study the LiCl concentration dependence of ion-water structures. The study reports the fractions of ion pairs and larger complexes as functions of concentration. Figure 4 shows remarkable agreement between the experiments and simulations. C_{fast} decreases in amplitude identically to the simulated fraction of ion pairs, and C_{slow} increases in amplitude identically to the simulated fraction of large clusters. Thus, the relationship between the dynamics and structures is confirmed.

Finally, the experimentally measured dynamics are able to elucidate the underlying cause of the increase in the bulk solution viscosity with increasing concentration. Figure 5 displays a plot of the viscosity versus the correlation time of the slow components of the dynamics. The correlation time is a measure of the average dynamical time scale. These results show that the viscosity is determined by the fraction of large ion-water complexes. As the concentration is increased, the concentration of large ion-water complexes increases. As the ion-water network grows, its structural dynamics slow. It is this slowing of the large ion-water large complex dynamics that is directly correlated with the increase in the viscosity.

■ ASSOCIATED CONTENT

Supporting Information

The Supporting Information is available free of charge at https://pubs.acs.org/doi/10.1021/acs.jpcb.3c01702.

Complete set of OHD-OKE decays of concentrated LiCl aqueous solutions (PDF)

■ AUTHOR INFORMATION

Corresponding Author

Michael D. Fayer − *Department of Chemistry, Stanford University, Stanford, California 94305, United States;* orcid.org/0000-0002-0021-1815; Phone: 650 723-4446; Email: fayer@stanford.edu

Author

Stephen J. Van Wyck − *Department of Chemistry, Stanford University, Stanford, California 94305, United States;* orcid.org/0000-0001-9011-9977

Complete contact information is available at: https://pubs.acs.org/10.1021/acs.jpcb.3c01702

Notes

The authors declare no competing financial interest.

■ ACKNOWLEDGMENTS

This work was supported by the National Science Foundation, Division of Chemistry, Award Number 1954392. S.J.V.W. acknowledges support from the National Science Foundation Graduate Research Fellowship Program.

■ REFERENCES

(1) Roedder, E. The Fluids in Salt. *Am. Mineral.* **1984**, *69*, 413−439.

(2) Jungwirth, P.; Cremer, P. S. Beyond Hofmeister. *Nat. Chem.* **2014**, *6*, 261−263.

(3) Oncsik, T.; Trefalt, G.; Borkovec, M.; Szilagyi, I. Specific Ion Effects on Particle Aggregation Induced by Monovalent Salts within the Hofmeister Series. *Langmuir* **2015**, *31*, 3799−3807.

(4) Roberts, S. T.; Ramasesha, K.; Tokmakoff, A. Structural Rearrangements in Water Viewed through Two-Dimensional Infrared Spectroscopy. *Acc. Chem. Res.* **2009**, *42*, 1239−1249.

(5) Palese, S.; Schilling, L.; Miller, R. D.; Staver, P. R.; Lotshaw, W. T. Femtosecond Optical Kerr Effect Studies of Water. *J. Phys. Chem.* **1994**, *98*, 6308−6316.

(6) Stirnemann, G.; Wernersson, E.; Jungwirth, P.; Laage, D. Mechanisms of Acceleration and Retardation of Water Dynamics by Ions. *J. Am. Chem. Soc.* **2013**, *135*, 11824−11831.

(7) Laage, D.; Stirnemann, G. Effect of Ions on Water Dynamics in Dilute and Concentrated Aqueous Salt Solutions. *J. Phys. Chem. B* **2019**, *123*, 3312−3324.

(8) Hribar, B.; Southall, N. T.; Vlachy, V.; Dill, K. A. How Ions Affect the Structure of Water. *J. Am. Chem. Soc.* **2002**, *124*, 12302−12311.

(9) Jiang, J.; Sandler, S. I. A New Model for the Viscosity of Electrolyte Solutions. *Ind. Eng. Chem. Res.* **2003**, *42*, 6267−6272.

(10) Gibbard, H. F., Jr.; Scatchard, G. Liquid-Vapor Equilibrium of Aqueous Lithium Chloride, from 25° to 100°C And from 1.0 to 18.5 Molal, and Related Properties. *J. Chem. Eng. Data* **1973**, *18*, 293−298.

(11) Suo, L.; Borodin, O.; Gao, T.; Olguin, M.; Ho, J.; Fan, X.; Luo, C.; Wang, C.; Xu, K. "Water-in-Salt"; Electrolyte Enables High-Voltage Aqueous Lithium-Ion Chemistries. *Science* **2015**, *350*, 938−943.

(12) Viola, W.; Andrew, T. L. An Aqueous Eutectic Electrolyte for Low-Cost, Safe Energy Storage with an Operational Temperature Range of 150 °C, from −70 to 80 °C. *J. Phys. Chem. C* **2021**, *125*, 246−251.

(13) Yamada, Y.; Usui, K.; Sodeyama, K.; Ko, S.; Tateyama, Y.; Yamada, A. Hydrate-Melt Electrolytes for High-Energy-Density Aqueous Batteries. *Nat. Energy* **2016**, *1*, 16129.

(14) Suo, L.; Borodin, O.; Wang, Y.; Rong, X.; Sun, W.; Fan, X.; Xu, S.; Schroeder, M. A.; Cresce, A. V.; Wang, F.; Yang, C.; Hu, Y. S.; Xu, K.; Wang, C. "Water-in-Salt" Electrolyte Makes Aqueous Sodium-Ion Battery Safe, Green, and Long-Lasting. *Adv. Energy Mater.* **2017**, *7*, No. 1701189.

(15) Smith, A. M.; Lee, A. A.; Perkin, S. The Electrostatic Screening Length in Concentrated Electrolytes Increases with Concentration. *J. Phys. Chem. Lett.* **2016**, *7*, 2157−2163.

(16) Chizhik, B. V. I. NMR Relaxation and Microstructure of Aqueous Electrolyte Solutions. *Mol. Phys.* **1997**, *90*, 653−659.

(17) Harsányi, I.; Pusztai, L. On the Structure of Aqueous LiCl Solutions. *J. Chem. Phys.* **2005**, *122*, 124512.

(18) Terpstra, P.; Combes, D.; Zwick, A. Effect of Salts on Dynamics of Water: A Raman Spectroscopy Study. *J. Chem. Phys.* **1990**, *92*, 65−70.

(19) Buchner, R.; Hefter, G. Interactions and Dynamics in Electrolyte Solutions by Dielectric Spectroscopy. *Phys. Chem. Chem. Phys.* **2009**, *11*, 8984−8999.

(20) Wachter, W.; Fernandez, Š.; Buchner, R.; Hefter, G. Ion Association and Hydration in Aqueous Solutions of LiCl and Li_2SO_4 by Dielectric Spectroscopy. *J. Phys. Chem. B* **2007**, *111*, 9010−9017.

(21) Barthel, J.; Hetzenauer, H.; Buchner, R. Dielectric Relaxation of Aqueous Electrolyte Solutions II. Ion-Pair Relaxation of 1:2, 2:1, and 2:2 Electrolytes. *Ber. Bunsen-Ges. Phys. Chem.* **1992**, *96*, 1424−1432.

(22) Tao, N. J.; Lindsay, S. M. Reorientational Relaxation of Water Molecules in LiCl Solution Studied by Depolarised Rayleigh Scattering. *J. Phys.: Condens. Matter* **1989**, *1*, 8709−8720.

(23) Roget, S. A.; Carter-Fenk, K. A.; Fayer, M. D. Water Dynamics and Structure of Highly Concentrated LiCl Solutions Investigated Using Ultrafast Infrared Spectroscopy. *J. Am. Chem. Soc.* **2022**, *144*, 4233−4243.

(24) Yuan, R.; Fayer, M. D. Dynamics of Water Molecules and Ions in Concentrated Lithium Chloride Solutions Probed with Ultrafast 2D IR Spectroscopy. *J. Phys. Chem. B* **2019**, *123*, 7628−7639.

(25) Lim, J.; Park, K.; Lee, H.; Kim, J.; Kwak, K.; Cho, M. Nanometric Water Channels in Water-in-Salt Lithium Ion Battery Electrolyte. *J. Am. Chem. Soc.* **2018**, *140*, 15661−15667.

(26) Lyashchenko, A. K.; Zasetsky, A. Y. Complex Dielectric Permittivity and Relaxation Parameters of Concentrated Aqueous Electrolyte Solutions in Millimeter and Centimeter Wavelength Ranges. *J. Mol. Liq.* **1998**, *77*, 61−75.
(27) Amo, Y.; Tominaga, Y. Dynamical Structure of Water in Aqueous Solutions of LiCl, NaCl, and KCl by Low-Frequency Raman Scattering: Comparison between the Multiple Random Telegraph Model and Cole-Cole Relaxation. *Phys. Rev. E* **1998**, *58*, 7553−7560.
(28) Tominaga, Y.; Wang, Y.; Fujiwara, A.; Mizoguchi, K. Dynamical Aspects of Water by Low-Frequency Raman Scattering. In *Studies in Physical and Theoretical Chemistry*, Nomura, H.; Kawaizumi, F.; Yarwood, J., Eds.; Elsevier: New York, 1995; Vol. *83*, pp. 187−194.
(29) Tao, N. J.; Li, G.; Chen, X.; Du, W. M.; Cummins, H. Z. Low-Frequency Raman-Scattering Study of the Liquid-Glass Transition in Aqueous Lithium Chloride Solutions. *Phys. Rev. A* **1991**, *44*, 6665−6676.
(30) Wei, Y. Z.; Sridhar, S. Dielectric Spectroscopy up to 20 GHz of LiCl/H_2O Solutions. *J. Chem. Phys.* **1990**, *92*, 923−928.
(31) Turton, D. A.; Corsaro, C.; Candelaresi, M.; Brownlie, A.; Seddon, K. R.; Mallamace, F.; Wynne, K. The Structure and Terahertz Dynamics of Water Confined in Nanoscale Pools in Salt Solutions. *Faraday Discuss.* **2011**, *150*, 493−504.
(32) Yuan, R.; Yan, C.; Fayer, M. Ion−Molecule Complex Dissociation and Formation Dynamics in LiCl Aqueous Solutions from 2D IR Spectroscopy. *J. Phys. Chem. B* **2018**, *122*, 10582−10592.
(33) Santa, I.; Foggi, P.; Righini, R.; Williams, J. H. Time-Resolved Optical Kerr Effect Measurements in Aqueous Ionic Solutions. *J. Phys. Chem.* **1994**, *98*, 7692−7701.
(34) Foggi, P.; Bellini, M.; Kien, D. P.; Vercuque, I.; Righini, R. Relaxation Dynamics of Water and HCl Aqueous Solutions Measured by Time-Resolved Optical Kerr Effect. *J. Phys. Chem. A* **1997**, *101*, 7029−7035.
(35) Heisler, I. A.; Mazur, K.; Meech, S. R. Low-Frequency Modes of Aqueous Alkali Halide Solutions: An Ultrafast Optical Kerr Effect Study. *J. Phys. Chem. B* **2011**, *115*, 1863−1873.
(36) Hou, M.; Lu, R.; Yu, A. Polarizability Series of Aqueous Polyatomic Anions Revealed by Femtosecond Kerr Effect Spectroscopy. *RSC Adv.* **2014**, *4*, 23078−23083.
(37) Bailey, H. E.; Wang, Y.-L.; Fayer, M. D. The Influence of Hydrophilicity on the Orientational Dynamics and Structures of Imidazolium-Based Ionic Liquid/Water Binary Mixtures. *J. Chem. Phys.* **2018**, *149*, No. 044501.
(38) Taschin, A.; Bartolini, P.; Eramo, R.; Righini, R.; Torre, R. Optical Kerr Effect of Liquid and Supercooled Water: The Experimental and Data Analysis Perspective. *J. Chem. Phys.* **2014**, *141*, No. 084507.
(39) Singh, B.; Dalvi, V. H.; Gaikar, V. G. Investigations of Clustering of Ions and Diffusivity in Concentrated Aqueous Solutions of Lithium Chloride by Molecular Dynamic Simulations. *RSC Adv.* **2015**, *5*, 15328−15337.
(40) Deeg, F. W.; Stankus, J. J.; Greenfield, S. R.; Newell, V. J.; Fayer, M. D. Anisotropic Reorientational Relaxation of Biphenyl: Transient Grating Optical Kerr Effect Measurements. *J. Chem. Phys.* **1989**, *90*, 6893−6902.
(41) Ruhman, S.; Williams, L. R.; Joly, A. G.; Kohler, B.; Nelson, K. A. Nonrelaxational Inertial Motion in Carbon Disulfide Liquid Observed by Femtosecond Time-Resolved Impulsive Stimulated Scattering. *J. Phys. Chem.* **1987**, *91*, 2237−2240.
(42) Yan, Y. X.; Nelson, K. A. Impulsive Stimulated Light Scattering I. General Theory. *J. Chem. Phys.* **1987**, *87*, 6240−6256.
(43) Sturlaugson, A. L.; Arima, A. Y.; Bailey, H. E.; Fayer, M. D. Orientational Dynamics in a Lyotropic Room Temperature Ionic Liquid. *J. Phys. Chem. B* **2013**, *117*, 14775−14784.
(44) Sturlaugson, A. L.; Fruchey, K. S.; Fayer, M. D. Orientational Dynamics of Room Temperature Ionic Liquid/Water Mixtures: Water-Induced Structure. *J. Phys. Chem. B* **2012**, *116*, 1777−1787.
(45) Sha, M.; Yamada, S. A.; Fayer, M. D. Orientational Pair Correlations and Local Structure of Benzonitrile from Molecular Dynamics Simulations with Comparisons to Experiments. *J. Phys. Chem. B* **2021**, *125*, 3163−3177.
(46) Fecko, C.; Eaves, J.; Tokmakoff, A. Isotropic and Anisotropic Raman Scattering from Molecular Liquids Measured by Spatially Masked Optical Kerr Effect Spectroscopy. *J. Chem. Phys.* **2002**, *117*, 1139−1154.
(47) Chang, Y. J.; Castner, E. W., Jr. Fast Responses from "Slowly Relaxing"Liquids: A Comparative Study of the Femtosecond Dynamics of Triacetin, Ethylene Glycol, and Water. *J. Chem. Phys.* **1993**, *99*, 7289−7299.
(48) Winkler, K.; Lindner, J.; Bürsing, H.; Vöhringer, P. Ultrafast Raman-Induced Kerr-Effect of Water: Single Molecule Versus Collective Motions. *J. Chem. Phys.* **2000**, *113*, 4674−4682.
(49) Scodinu, A.; Fourkas, J. T. Comparison of the Orientational Dynamics of Water Confined in Hydrophobic and Hydrophilic Nanopores. *J. Phys. Chem. B* **2002**, *106*, 10292−10295.
(50) Wiewior, P. P.; Shirota, H.; Castner, E. W., Jr. Aqueous Dimethyl Sulfoxide Solutions: Inter-and Intra-Molecular Dynamics. *J. Chem. Phys.* **2002**, *116*, 4643−4654.
(51) Castner, E., Jr.; Chang, Y.; Chu, Y.; Walrafen, G. The Intermolecular Dynamics of Liquid Water. *J. Chem. Phys.* **1995**, *102*, 653−659.
(52) Palese, S.; Buontempo, J. T.; Schilling, L.; Lotshaw, W. T.; Tanimura, Y.; Mukamel, S.; Miller, R. D. Femtosecond Two-Dimensional Raman Spectroscopy of Liquid Water. *J. Phys. Chem.* **1994**, *98*, 12466−12470.
(53) Saito, S.; Ohmine, I. Third Order Nonlinear Response of Liquid Water. *J. Chem. Phys.* **1997**, *106*, 4889−4893.
(54) Ratajska-Gadomska, B.; Białkowski, B.; Gadomski, W.; Radzewicz, C. Ultrashort Memory of the Quasicrystalline Order in Water by Optical Kerr Effect Spectroscopy. *Chem. Phys. Lett.* **2006**, *429*, 575−580.
(55) Torre, R.; Bartolini, P.; Righini, R. Structural Relaxation in Supercooled Water by Time-Resolved Spectroscopy. *Nature* **2004**, *428*, 296−299.
(56) Taschin, A.; Bartolini, P.; Fanetti, S.; Lapini, A.; Citroni, M.; Righini, R.; Bini, R.; Torre, R. Pressure Effects on Water Dynamics by Time-Resolved Optical Kerr Effect. *J. Phys. Chem. Lett.* **2020**, *11*, 3063−3068.
(57) Taschin, A.; Bartolini, P.; Eramo, R.; Righini, R.; Torre, R. Evidence of Two Distinct Local Structures of Water from Ambient to Supercooled Conditions. *Nat. Commun.* **2013**, *4*, 2401.
(58) Turton, D. A.; Corsaro, C.; Martin, D. F.; Mallamace, F.; Wynne, K. The Dynamic Crossover in Water Does Not Require Bulk Water. *Phys. Chem. Chem. Phys.* **2012**, *14*, 8067−8073.
(59) Asbury, J. B.; Steinel, T.; Stromberg, C.; Corcelli, S. A.; Lawrence, C. P.; Skinner, J. L.; Fayer, M. D. Water Dynamics: Vibrational Echo Correlation Spectroscopy and Comparison to Molecular Dynamics Simulations. *J. Phys. Chem. A* **2004**, *108*, 1107−1119.
(60) Asbury, J. B.; Steinel, T.; Kwak, K.; Corcelli, S. A.; Lawrence, C. P.; Skinner, J. L.; Fayer, M. D. Dynamics of Water Probed with Vibrational Echo Correlation Spectroscopy. *J. Chem. Phys.* **2004**, *121*, 12431−12446.
(61) Yan, C.; Kramer, P. L.; Yuan, R.; Fayer, M. D. Water Dynamics in Polyacrylamide Hydrogels. *J. Am. Chem. Soc.* **2018**, *140*, 9466−9477.
(62) Smirnov, P. R.; Trostin, V. N. Structure of the Nearest Surrounding of the Li+ Ion in Aqueous Solutions of Its Salts. *Russ. J. Gen. Chem.* **2006**, *76*, 175−182.
(63) Pethes, I. The Structure of Aqueous Lithium Chloride Solutions at High Concentrations as Revealed by a Comparison of Classical Interatomic Potential Models. *J. Mol. Liq.* **2018**, *264*, 179−197.
(64) Mao, S.; Duan, Z. The Viscosity of Aqueous Alkali-Chloride Solutions up to 623 k, 1,000 bar, and High Ionic Strength. *Int. J. Thermophys.* **2009**, *30*, 1510−1523.

https://doi.org/10.1021/acs.jpcb.3c01702
J. Phys. Chem. B 2023, 127, 3488−3495